A new heat transfer model for engines with tumble motion

Pablo Olmeda, Jaime Martín*, Ricardo Novella, Ricardo Carreño

CMT-Motores Térmicos, Universitat Politècnica de València, Camino de Vera s/n, 46022, Valencia, Spain

Abstract

In the last years, a growing interest about increasing the engine efficiency has led to the development of new engine technologies. The accurate determination of the heat transfer across the combustion chamber walls is highly relevant to perform a valid thermal balance while evaluating the potential of new engine concepts. Several works dealing with heat transfer correlations that consider the swirl motion are found in the literature; however, there is a lack of works dealing with heat transfer correlations which take into account the effect of the tumble movement. In this work, a new heat transfer model accounting for the tumble motion is presented. A two stroke HSDI Diesel engine with high tumble and no swirl is used to perform the theoretical study, the model development and its final calibration. Initially, a theoretical analysis of the gas movement phenomena is carried out based on CFD results and then, a model is developed and calibrated based on a skip-fire testing technique. Finally, a sensitivity study focused on evaluating the model robustness is performed. The results confirm an average RMSE reduction of 70% with respect to the Woschni model, being this consistent improvement qualitatively evidenced in the instantaneous heat transfer evolution.

Keywords: Combustion Diagnosis, Engine Heat Transfer, Tumble

*Corresponding author. Tel: +34963877650; fax: +34963877659
Email address: jaimardi@mot.upv.es (Jaime Martín)
URL: www.cmt.upv.es (Jaime Martín)

Nomenclature

α	Crank Angle	[°]
c_m	Piston mean speed	$[m/s]$
c_u	Tangential vortex speed	$[m/s]$
D	Cylinder diameter	$[m]$
ρ	Density	$[kg/m^3]$
$\Delta\alpha$	Angular duration	[°]
γ	Adiabatic exponent	[-]
h	Heat transfer coefficient	$[J/kg]$
η_{tr}	Trapping ratio	[-]
k	Conductivity	$[W/mK]$
$\dot{m}$	Mass flow rate	$[kg/s]$
p	In-cylinder pressure	$[bar]$
Q	Accumulated heat transfer	$[kW]$
$\dot{Q}$	Heat transfer rate	$[J/°]$
R	Specific gas constant	$[J/kgK]$
RoHR	Rate of Heat Release	$[J/°]$
S	Engine stroke	$[m]$
T	Temperature	$[K]$, $[°C]$
V	Volume	$[m^3]$
v	Velocity	$[m/s]$
μ	Dynamic viscosity	$[P_a s]$

Abbreviations

ATDC	After Top Dead Centre
BDC	Bottom Dead Centre
BTDC	before Top Dead Centre
CFD	Computational Fluid Dynamics
CI	Compression Ignition
EGR	Exhaust Gas Recirculation
HCCI	Homogeneous Charge Compression Ignition
HSDI	High Speed Direct Injection
HT	Heat Transfer
ICE	Internal Combustion Engine
IGR	Internal Gas Recirculation
IVC	Intake Valve Closing
IVO	Intake Valve Opening
PCCI	Premixed Charge Compression Ignition
SI	Spark Ignition
TDC	Top Dead Centre
TR	Tumble Ratio

1. Introduction

The global awareness towards the greenhouse gases emissions has led to a more stringent ICE emissions legislation, thus focusing the automotive researchers and manufacturers attention on the development of cleaner and more efficient powertrains. In the last years, the efforts have been mainly focused on the reduction of the NO_x and soot emissions by means of different injection strategies [1], high pressure fuel injection systems [2], multiple injections [3], high boost pressure [4], exhaust gases recirculation (EGR) [5], variable valve timing [6], high swirl [7, 8] and tumble ratios [9], new clean fuels [10, 11] or after treatment systems [12]. Nowadays, there is an increasing interest towards the optimization of the fuel consumption, and hence the reduction of the CO_2 emissions [13]. To comply with the upcoming requirements, new combustion concepts such as HCCI [14] and PCCI [15], and new automotive engine concepts such as downsizing [16, 17], and two-stroke engines [18] are in the centre of the research. The air management is a common factor in these works, since it is a key issue to improve the air-fuel mixing process and achieve faster burning rates [19], and therefore modern ICE are designed to generate high vorticity and turbulence in the combustion chamber.

There are several methodologies aimed at the evaluation of specific engine technologies or operation strategies, being some of the most widespread the combustion diagnosis based on in-cylinder pressure evolution [20] and the energy balances [21]. On the one hand, the combustion diagnosis evaluates the combustion performance by analysing the rate of heat released (RoHR), which is obtained by solving the first law of thermodynamics and the equation of state [22]. On the other hand, the energy balance determines the chemical fuel energy distribution in the different engine subsystems, being the most important terms the brake power, the exhaust gases energy and the heat transfer from the combustion chamber [19]. Thus, it is evident that both methodologies requires the accurate determination of the heat transfer (HT) across the combustion chamber walls, which can be carried out either by experimental or modelling methodologies. The main drawback for the experimental determination is the necessity of a special instrumentation, usually not available in a standard test bench [21]. Therefore, the HT modelling is interesting as an alternative approach, whose complexity and time consuming depends on the specific application.

The aforementioned applications demand HT models with low computational effort (with time consumption of minutes or even seconds). Thus, a lot of proposals dealing with the HT estimation in ICE can be found in the literature for both, compression ignition (CI) and spark ignition (SI) engines. Some of the most widespread correlations for HT coefficient calculation are those based on the well-known Woschni [23], Annand [24] and Hohenberg [25] works. To make these models suitable for a specific application, they must be adjusted based on different techniques such as CFD modelling [26], experimental measurements [27, 28], or thermodynamic assumptions [29]. In general, these models correlate the HT coefficient with the thermodynamic state of the gases (pressure and temperature), the engine geometry (bore and stroke) and the gas movement (gas velocity and flow pattern), being this last parameter the most difficult to asses due to the unsteady nature of the gas motion, since it is a turbulent 3D flow with no clear symmetry of the gas properties along the chamber.

The main rotative macro structures that can be found in ICE are the swirl and tumble, being differentiated by their rotary axis (swirl rotates in the cylinder axis and tumble in the diametrical axis). Both are generated during the intake process and evolve in the compression-expansion stroke thanks to the engine geometry (particularly ports and combustion chamber configuration). The swirl movement is prompted by chamber configurations consisting of a shallow bowl engraved into the piston crown [19], whilst the tumble movement is enhanced by pentroof combustion chambers [30, 31]. The swirl characteristics have been widely studied, and most of the HT correlations include a term accounting for its contribution to the characteristic gas velocity used to calculate the HT coefficient [23, 26]. However, there is a lack of HT correlations dealing with the effect of the tumble characteristics on the HT coefficient. The tumble is usually evaluated by means of experimental techniques such as LDV and PIV [32, 33], involving several engine modifications, or CFD modelling [34, 35] leading to a long computational time. Alternatively, there are some quasi-dimensional models [30, 36], which are faster than the CFD models, but require a detailed knowledge of the fluid motion pattern and also of the engine ports and combustion chamber geometry. This specific information is not usually available for combustion diagnosis, and hence leads to a lack of generality of the models for be applied to in different engines.

In this work, a generally applicable HT model that includes the gas velocity evolution produced by a high tumble movement is proposed. For the model development, a research CI two-stroke HSDI engine with high tumble motion and no swirl was experimentally characterized. The fluid motion analysis and model development was carried out on the basis of CFD simulations, whereas the calibration of the model was carried out in a specific experimental installation, specially developed to perform skip-fire tests.

2. Methodology

The objective of this work is the determination of a semi-empirical HT model, which takes into account the tumble flow motion pattern in the combustion chamber. The model was developed following three main stages as shown in Figure 1. In the next paragraph, the definition of each step are explained:

– Theoretical analysis: a well-grounding model requires a first deep understanding of the phenomena involved, and thus a comprehensive bibliography review regarding the tumble generation and dissipation processes, and the influence of the geometrical and operating parameters was carried out. In order to analyse the instantaneous gas evolution in the specific engine under investigation, CFD simulations of the complete skip-fire cycle were used. The results are discussed in detail with the aim of identifying the operating parameters that must be taken into account by the model.

– Model development: starting from the CFD results, a semi-empirical model able to reproduce the gas velocity dissipation was developed. The model must be suitable for combustion diagnosis, and therefore it considers the main mechanisms involved in the tumble generation (geometry and operating conditions), but is still simple and keeps low computational cost in terms of power and time. The input parameters required, consist mainly of those mean values generally acquired in a test bench.

– Model calibration: this stage was carried out based on skip-fire measurements, which consist of skipping the injection of one cycle, thus obtaining a motoring measurement with the air management of a conventional combustion. The calibration focuses on the determination of the fitting constant values, with the objective of reducing the difference between the experimental HT (obtained through the application of the first law in the combustion chamber) and the modelled HT. The skip-fire tests are used instead of motoring measurements to reproduce a realistic intake process, being this specially important to ensure the scavenging process in two-stroke engines [37, 38], and also to have the same thermal properties (temperatures and gas composition) in the chamber than those of a conventional combustion operation, being this critical for the HT process.

Once the model is calibrated, it is compared with a model widely accepted as a reference by the scientific community. For this purpose, the Woschni HT model [23, 39], which has been widely evaluated [40] and used as a start point in several works [26, 27] has been selected. The objective is to evaluate the effect of the tumble gas velocity evolution on HT. Finally, a sensitivity study is carried out with the objective of evaluating its robustness against the effects of possible experimental and calibration uncertainties, being this information important when the model is transferred to different engines.

3. Experimental and Theoretical tools

A research single-cylinder engine, with high tumble induction and no swirl was selected to perform the CFD simulations and the experimental tests. Initially, the engine architecture and the test cell characteristics are described. Subsequently, the details of the CFD simulation, along with the model validation are discussed.

3.1. Engine architecture and hardware

The experimental activities were performed on a single-cylinder, research version of a 2-stroke HSDI diesel engine prototype. The main engine geometrical characteristics are presented in Table 1. The cylinder head and combustion chamber geometry, shown in Figure 2, were completely adapted to ensure a suitable in-cylinder flow pattern, in order to optimize the scavenging of burnt gases and to reduce the short-circuit losses of fresh air going directly from the intake into the exhaust ports. The cylinder head geometry presents a staged roof for baffling the flow of air between the intake and exhaust valves, forcing the air to follow the path of the cylinder wall toward the bottom of the cylinder. This geometry provides the best compromise between scavenging efficiency, acceptable permeability, and convenient combustion chamber geometry [18].

The engine is equipped with an hydraulic cam-driven variable valve timing system, allowing a flexibility of 30° on both intake and exhaust valve timings independently from the mechanical cam timing. The optimum camshaft configuration, presented in Table1, was experimentally defined by testing different opening durations and maximum lifts in a medium load and medium speed operating point. The trapping ratio η_{tr} was experimentally determined by means of a tracer gas method [41, 42]. It consist on injecting a controlled quantity of CH_4 (tracer gas) along with the intake flow, and then measure the CH_4 concentration at the intake and exhaust manifolds. It is assumed that the CH_4 is homogeneous mixed with the intake air, and the mass trapped in the cylinder was completely burn during combustion, therefore the CH_4 ratio at intake and exhaust is an indicator of the short-circuited air mass. Thus, an accurate estimation of the short-circuited mass was performed by means of mass balances at the intake, exhaust and in-cylinder gases.

The total trapped mass in the cylinder is a key issue to accurately obtain the IVC thermodynamic conditions, required for both CFD calculations and experimental HT determination. It is given by the addition of the trapped air mass after the IVC, and the internal gas recirculation (IGR), defined as the fraction of residual gases retained from the previous combustion cycle in the total trapped mass in the cylinder. The effective air/fuel ratio is calculated from the mass of usable air available in the trapped charge, excluding the air in the IGR since it is not really usable, divided by the injected fuel mass. The IGR ratio and the total trapped mass are estimated using simplified thermodynamic calculations. This estimation is based on an enthalpy balance, where the enthalpy of the total trapped mass at the IVC equals to the enthalpy of the residual mass plus the enthalpy of the intake delivered trapped mass (fresh air plus external EGR), both estimated also at the IVC.

3.2. Test cell characteristics

The engine was assembled into a fully instrumented test cell, whose scheme is shown in Figure 3. The engine is fed with the compressed air provided by an external compressor, which operation was set to simulate boost conditions. A throttle valve located at the exhaust line after the exhaust settling chamber is used to simulate the back-pressure that would be produced by the turbine. The experimental cell also includes a low pressure EGR system, designed to provide arbitrary levels of cooled EGR even at very high intake boost pressures. Water and oil cooling circuits are also independent from the engine, and temperatures are strictly controlled and monitored during all the experimental tests. The fuel consumption of the engine is measured with a gravimetric dynamic fuel meter.

Pollutant emissions from the engine are sampled in the exhaust line, close to the exhaust settling chamber and routed to a state-of-the-art gas analyser by a heated pipe to ensure gas temperatures above 150 °C. Measurements of CO_2 at intake and exhaust (to determine the EGR rate) are performed for all the tests, and a dedicated CH_4 analyser is used to trace both intake and exhaust CH_4 concentrations when performing η_{tr} measurements. Most relevant averaged test cell and engine parameters, pollutant emissions, and high frequency instantaneous signals are recorded using a dedicated data acquisition system. The high frequency signals are acquired using an oscilloscope synchronized with an optical angular encoder with a resolution of 0.2°. The cylinder pressure is measured using a piezoelectric sensor, while a piezo-resistive pressure sensor is placed at the cylinder liner near to the BDC, with the objective of reference the piezoelectric sensor differential pressure signal. The combustion diagnosis and the determination of relevant parameters such as: indicated mean effective pressure (imep), combustion phasing, maximum cylinder pressure, rate of heat release (RoHR), etc. are calculated from the in-cylinder pressure by means of an in-house combustion diagnosis software named CALMEC [22, 43].

To perform the skip-fire test, a special electronic device consisting of an electronic controlling box and a dummy injector was implemented. Its operation consist on deviating a injection command pulse to the dummy injector every determined number of injections; therefore, there is no injection nor combustion in the cycle, thus obtaining a motoring test with the same thermal, intake and scavenging process of a nominal combustion cycle. The main drawback of the skip-fire is that once a combustion is skipped, the following cycles are faulty, which results in abnormal combustion or even in misfire. This issue is solved by waiting until the engine operation returns to normality, which occurs about 5 cycles after the skip-fire cycle, as can be seen in Figure 4. In this work, 15 cycles (14 combustion and 1 motoring) were measured to ensure complete engine stabilization. Since 20 cycles are required in order to have a confident averaged cycle [20], the measurement of 300 cycles is required.

The experiments performed consist on a combination of engine speed and $\Delta p = p_{in} - p_{out}$ sweeps, being p_{in} and p_{out} the inlet and outlet pressures. These parameters were varied owing to their major influence on the intake and scavenging processes, i.e. low speed and Δp implies longer intake time but also lower air flow rate at intake, on the counterpart, high speed and Δp has the opposite effect. The combination of the effects of these parameters are related with the scavenging efficiency of the exhaust gases and the short-circuit. Therefore, the engine speeds tested are 1200, 1500 and 1800 rpm and Δp are 300, 400 and 500 *mbar*. The complete experimental matrix is presented in Table 2. It provides a complete data base of the engine operating conditions, which allows performing a further calibration of the model that optimise the results in a wide operating range.

3.3. CFD model

The computational model was built in the CONVERGE CFD platform. Full coupled open and closed cycle computations using the full intake/exhaust and cylinder geometries were carried out since the combustion chamber is non-symmetric. The computational domain at the intake valve closing (IVC) angle is shown in the left plot from Figure 2. The CFD code uses a structured Cartesian grid with base cell size of 3 mm. Three additional grid refinements linked to flow velocity and temperature were performed by means of an adaptive mesh refinement as well as a fixed three level refinement within the spray region.

The injection rate profile was generated from the experimental database available after the injector characterization (mass flow rate and spray momentum flux) performed in dedicated test rigs. The diesel injection is simulated by the standard Droplet Discrete Model. Diesel fuel physical properties are defined using Diesel 2 as surrogate. Spray atomization and break-up are simulated by means of the KH-RT model. Turbulent flow is modelled by means of the RNG $k - \varepsilon$ model with wall-functions in order to account for wall heat transfer. Concerning combustion modelling, a direct integration of detailed chemistry approach was used by means of the CONVERGE code and the SAGE solver. Finally, the chemical properties of Diesel fuel are defined using n-heptane as surrogate.

The set-up and validation of the CFD model was performed at the reference case (see Figure 5), operating with the conventional Diesel combustion concept. The quality of the model was evaluated by comparing its combustion and emissions results with those obtained experimentally in the engine as presented in Table 3. Figure 5 shows the comparison between the CFD and experimental cylinder pressure and RoHR profiles. The CFD model performance is considered as suitable for being used along the evaluation of the gas flow motion within the chamber as well as the HT from the gas to the combustion chamber walls.

In order to increase the weight of the tumble motion on the HT, the original engine configuration was adapted for the CFD calculation: aluminium was set as the piston material because its higher conductivity than steel, and the intake settings were defined to enhance the tumble generation, achieving higher tumble ratios and subsequently higher HT than the original configuration.

4. Theoretical analysis

The theoretical analysis starts with the description of the reference HT model, with the objective of identifying how it considers the instantaneous gas velocity to calculate the HT evolution. Then, the main tumble generation process according to the literature is presented, followed by the specific CFD simulation of the engine used for the model development.

4.1. Reference heat transfer model

The HT to the combustion chamber walls in motoring or skip-fire tests (or during the compression stroke and after the end of combustion) is essentially governed by convection, even though gas radiation to the walls also occurs, its weight is negligible at these conditions in comparison with convection [24]. On the contrary, the radiation gain relevance in combustion measurements since the formation of soot particles at high temperatures increases the radiation emission. There is no general agreement with respect to the fraction of the HT that is transferred by radiation, Morel and Keribar [44] obtained values ranging from 4% to 20%, whereas Heywood [19] states that this fraction can be higher than 20%. An accurate radiative model requires the calculation of the soot formed in the spray [45]; therefore, it is usual to consider a HT coefficient that accounts for convection and radiation together.

The convective HT is determined by means of the Newton's law of cooling $Q = hA(T_g - T_w)$, where h is the heat transfer coefficient, A is the heat transfer surface area (i.e. the instantaneous combustion chamber area), and T and T_w are the spatially averaged gas and walls temperatures (i.e. piston, piston head and cylinder liner temperatures). The A value is geometrically defined, being its instantaneous value obtained from the kinematic analysis of the mechanism. T_g is estimated from the in-cylinder pressure, the ideal gas law and the trapped mass, meanwhile T_w requires specific models to their determination [20]. In this work, the trapped mass is determined by means of the mass balance described in Section 3.1, and T_w by means of a conductance lumped model [46, 47].

One of the most scientifically accepted expressions for the h determination is the Woschni correlation [23, 39]. Woschni developed his model based on a dimensional analysis, where the relation between the Nusselt, Reynolds and Prandtl numbers (N_u, R_e and P_r respectively) is defined as:

$$N_u = a\, R_e^b\, P_r^c \tag{1}$$

being a, b and c constants. N_u and R_e are expressed in terms of the engine geometry and gas properties as $N_u = \frac{hD}{k_g}$ and $R_e = \frac{\rho_g D v_g}{\mu_g}$, where D is the engine bore, k_g, ρ_g, v_g and μ_g are the conductivity, the density, the gas velocity and the dynamic viscosity of the gas respectively. k_g and μ_g depends on gas temperature according to $k_g \propto T_g^{0.75}$ and $\mu_g \propto T_g^{0.62}$. P_r of the air has a value about 0.7 in the working temperature range within the combustion chamber, thus P_r^c is usually considered constant. Rearranging in Equation 1, Equation 2 is obtained:

$$h = C\, D^{-0.2}\, p^{0.8}\, T_g^{-0.55}\, v_g^{0.8} \tag{2}$$

where C is a constant value, and the gas velocity is determined as:

$$v_g = C_{w1} c_m + C_{w2} c_u + C_2 \frac{V_d T_{IVC}}{V_{IVC} p_{IVC}} (p - p_0) \tag{3}$$

being C_{w1}, C_{w2} and C_2 constant values, c_m the mean piston speed, V_d the displaced volume, T_{IVC}, V_{IVC}, p_{IVC} the temperature, volume and pressure at IVC respectively, p is the instantaneous pressure and p_0 is the motoring pressure, obtained by assuming a polytropic evolution (note that in motoring conditions $p \equiv p_0$) and c_u is the tangential speed generated by the swirl vortex, which is defined as $c_u = \pi D N_T$, where swirl vortex frequency N_T is experimentally determined.

In the original Woschni equation, the c_u value was considered as constant. The reference model used in this work accounts for the impact of the instantaneous evolution of the swirl over c_u by means of a trigonometric function [26], which simulates the vortex acceleration due to the upward piston movement.

4.2. *Tumble formation, evolution and dissipation*

The determination of the specific generation and dissipation timing as well as the mechanisms that enhance or reduce the vortex formation requires dedicated experimental techniques [32, 33] or CFD simulations [34, 35]. Moreover, the tumble characteristics depend on the engine geometry and the operating conditions; however, there is a general agreement regarding the main process. The vortex formation starts few crank angle degrees after the IVO, when the high speed air goes into the chamber. Due to the combustion chamber geometry, the air is forced to sweep the wall and tries to form a small vortex; however, at this stage the piston is in the proximities of the TDC and the small size of the combustion chamber is not enough to stand for the vortex formation. In the early intake process (scavenging process in two-stroke engines), both intake and exhaust valves are simultaneously opened, thus some air is short-circuited as shown in Figure 6a, which also goes in detriment of the tumble generation. Figure 6b shows how during the intake stroke a small vortex is generated and continuously accelerated thanks to the angular moment added by the incoming air, this process lasts until the IVC, as shown in Figure 6c. The completely developed vortex is then accelerated along the compression stroke as a result of the angular momentum conservation (since the vortex radius decreases). At some stage of the compression stroke, the tumble is completely dissipated by the effect of friction with the wall and the increasingly smaller vortex radius, which forces the formation of turbulent micro-structures as depicted in Figure 6d.

Regardless the specific application, the gas movement inside the chamber has a major importance in the HT coefficient calculation since the high rotational speed increases the HT before the TDC. Once the tumble dissipates, the resulting high turbulence still contributes in a smaller extent to the HT, extending the gas velocity influence several degrees after the TDC. It is interesting to highlight that, contrary to the tumble, the swirl is considered to be accelerated in the compression stroke, and decelerated similarly in the expansion stroke, resulting in a symmetrical effect on the HT. Thus, the most general swirl models cannot accurately determine the effect of the gas velocity on the HT for engines with tumble, being necessary a model that considers the instantaneous evolution of the spatially averaged gas velocity, taking into account the previous discussed characteristics. This objective is achieved in this work, based on simplifications of the more complex 3D phenomena described in the next section.

4.3. *CFD results analysis*

The main features of the tumble motion can be identified in Figure 7, where the tumble ratio (TR) in the X-Y plane (defined in Figure 6a) is sketched. Results obtained confirms how the TR in the Z-Y plane and the swirl ratio (SR) in the X-Z plane are negligible. Figure 7 shows that the tumble formation begins in the piston upward stroke about 175° BTDC, reaching its maximum around 130° BTDC (before the IVC). It means that the tumble dissipation starts in the compression stroke, which is in accordance with that found in the literature [32]. The tumble is completely dissipated close to TDC, however, the TR value is close the zero several degrees before the TDC as observed in the detail presented in Figure 7.

Higher TR boost the HT from the gases to the walls by increasing the value of the last term in Equation 2. In Figure 8, the HT obtained in the CFD simulations ($\dot{Q}_{CFD}$) is presented, along with a HT calculated accounting only for the piston speed term ($\dot{Q}_{c_m}$), but neither swirl nor tumble. $\dot{Q}_{c_m}$ is calculated by adjusting the constant C_{w1} of Equation 3 in the expansion stroke, keeping $c_u = 0$. This step was performed to assess the effect of the vortex (swirl or tumble) on the HT, by determining the spatially averaged gas velocity. The CFD spatially averaged gas velocity (v_{CFD}) presented in Figure 8 is the velocity generated by the tumble vortex. It is calculated from a HT coefficient h' obtained from the difference between $\dot{Q}_{CFD}$ and $\dot{Q}_{c_m}$ as presented in Equation 4, then v_{CFD} is obtained by combining Equations 4 and 2 as presented in Equation 5. It is interesting to notice how the v_{CFD} presented in Figure 8 becomes zero near to 30° ATDC, although the tumble has been completely dissipated. This can be explained by the turbulence generated as result of the tumble destruction, which has an important effect in the HT coefficient since it occurs in the proximities of the TDC, where the in-cylinder pressure and the temperature difference between gas and walls are the highest.

$$h' = \frac{\dot{Q}_{CFD} - \dot{Q}_{c_m}}{A} \tag{4}$$

$$v_{CFD} = \sqrt[0.8]{\frac{h'}{C\ D^2\ p^{0.8}\ T^{-0.55}}} \tag{5}$$

The results obtained from the CFD model regarding the description of the shape of v_{CFD}, allows the development of a HT model that accounts for the instantaneous tumble velocity characteristics. The HT model proposed in this work is detailed described in the following section.

5. Model development

The last term in Equation 2 corresponding to the gas velocity v_g, is replaced by a tumble-generated gas velocity v_t, which is assumed to be proportional to a characteristic gas mean velocity $\bar{v}_m$ during the intake process, a tumble gas velocity dissipation function f_w and the mean piston speed c_m as follows:

$$v_t = C_{t1}\ \bar{v}_m\ f_w + C_{t2}\ c_m + C_2\ \frac{V_d T_{IVC}}{V_{IVC} p_{IVC}}\ (p - p_0) \tag{6}$$

where C_{t1} and C_{t2} are proportionality constants affecting f_w and c_m respectively. Starting from the results obtained for the gas velocity in the CFD simulations, it was found that an exponential Wiebe-like function (Equation 7) suitably follows the trend observed for the tumble gas velocity.

$$f_w(\alpha) = exp^{a(\frac{\alpha-\alpha_0}{\alpha_f-\alpha_0})^m} \tag{7}$$

where f_w is a S-shape function, with values between 0 and 1, m is a fitting constant used to adjust the shape, α is the crank angle, α_0 and α_f are angles related to the begin and the end of the gas velocity dissipation process, and $a = -6.907$ is a constant value, adjusted to ensure a v_t dissipation of 99.9% at $\alpha = \alpha_f$.

Considering the parameters that can affect the vortex formation, a mean gas velocity during the intake process $\bar{v}_m$ was defined in Equation 8. It takes into account the air mass going into the cylinder $\dot{m}_a$, the intake process duration $\Delta\alpha_{IVO-IVC}$, the mean air density during the intake process $\bar{\rho}_a$, the trapping efficiency η_{tr} and the effective intake valve area A_{eff}.

$$\bar{v}_m = \frac{360\ \eta_{tr}\ \dot{m}_a}{A_{eff}\ \bar{\rho}_a\ \Delta\alpha_{IVO-IVC}} \tag{8}$$

where $\bar{\rho}_a$ was calculated considering a mean gas in-cylinder temperature $\bar{T}_{cyl,int}$, estimated assuming an adiabatic process between the intake and the cylinder as follows:

$$\bar{T}_{cyl,int} = \bar{T}_{int}\left(\frac{\bar{p}_{cyl,int}}{\bar{p}_{int}}\right)^{\frac{\gamma-1}{\gamma}} \tag{9}$$

where $\bar{T}_{int}$ and $\bar{p}_{int}$ are the mean temperature and pressure at the intake settling chamber, $\bar{p}_{cyl,int}$ is the mean in-cylinder pressure during the intake process and γ is the adiabatic gas constant. Finally, the instantaneous gas velocity v_t is defined in Equation 10, which was determined by combining Equation 6, Equation 7 and Equation 8.

$$v_t(\alpha) = C_{t1}\ \bar{v}_m\ exp^{-6.907(\frac{\alpha-\alpha_0}{\alpha_f-\alpha_0})^m} + C_{t2}\ c_m + C_2\frac{V_d T_{IVC}}{V_{IVC} p_{IVC}}(p - p_0) \tag{10}$$

6. Model calibration and sensitivity analysis

6.1. Model calibration

The calibration of C_{t1} and C_{t2} was carried out on the basis of the RoHR error reduction in a set of skip-fire tests, following an adjustment methodology presented in a previous work [48]. The use of skip-fire cycles avoids the combustion uncertainties, therefore the term in the right of the Equation 10, related with the pressure increment due to combustion equals to zero. Moreover, the criteria of RoHR error reduction in skip-fire test used to adjust C_{t1} and C_{t2} is equivalent to the reduction in the difference between the experimental and the modelled HT.

The model calibration consisted of the determination of the function shape parameters (i.e. α_0, α_1 and m) and the proportionality constants (i.e. C_{t1} and C_{t2}). In order to assure the model stability and generality, a constant ratio $r_t = C_{t1}/C_{t2}$ was defined. This ratio is defined since the increase of variables to be adjusted could result in undesired behaviour and non-convergence. After the calibration process, the final adjusted values are included in Table 4.

The CFD gas velocity and the model gas velocity are compared in Figure 9 along with the resulting heat transfer for an operating point at 1500 rpm and Δp of 450 mbar. As can be seen, the CFD and the proposed model gas velocities are in good agreement, being remarkable how the model follows the CFD gas velocity trend. However, there are some differences between the gas velocity obtained from the CFD and the model, mainly due to the adjustment criteria which takes into account the RoHR instead of the gas velocity itself. This criteria was selected because the final objective is to accurately calculate the HT, therefore the HT adjustment observed in Figure 9 is better than that of the gas velocity, which indicates the model potential for considering the tumble phenomena and finally for estimating the HT.

The comparison between the experimental HT ($\dot{Q}_n$), the HT calculated using the reference Woschni model ($\dot{Q}_w$), whose constants in Equation 3 were calibrated for the engine tested, and the HT estimated using the model developed in this work ($\dot{Q}_t$) is presented in Figure 10. For the sake of simplicity, Figure 10 presents the medium Δp operation points of each engine speed. It is evident how $\dot{Q}_t$ provides a better fit with $\dot{Q}_n$ than $\dot{Q}_w$, and some qualitative and quantitative remarks can be underlined:

– Low discrepancy is observed between the instantaneous evolution of $\dot{Q}_n$ and $\dot{Q}_t$, which indicates that in the studied cases, v_t accounts well for the spatially averaged gas velocity. The good agreement between the maximum $\dot{Q}_n$ and $\dot{Q}_t$ observed in Figure 10 indicates that $\bar{v}_m$ can retain the information regarding the operating condition variations. Moreover, the C_{t1} value close to 1 indicates that $\bar{v}_m$ is also representative of the maximum gas velocity in the combustion chamber.

– In motoring tests, the swirl-model used in Equation 3 assumes that the vortex is accelerated in the compression stroke, and since no friction between gas and walls is considered, the vortex is symmetrically decelerated in the expansion stroke. Therefore, $\dot{Q}_w$ is almost symmetric with respect to the TDC, with its maximum value few degrees BTDC. The slight asymmetry of $\dot{Q}_w$ is caused by the effect of the higher pressure and temperature BTDC in the HT estimation (see Equation 2). In the case of $\dot{Q}_t$, the maximum value is reached several degrees BTDC which is more reasonable, considering the mechanism of the tumble dissipation explained in Section 4.2.

– The RMSE of the complete experimental matrix is included in Table 5. It is observed how the uncertainty of $\dot{Q}_t$ is remarkably lower than that of $\dot{Q}_w$ in all the cases, showing an average improvement of about 70%. This corroborates the better performance of the proposed model in all the operating range. In the particular case of 1800 rpm and Δp of 500 mbar, the uncertainty reduction of $\dot{Q}_t$ is lower than in the rest of the operating points (about 40%), this is probably due to the higher experimental uncertainty at this operating condition, since this point shows the highest noise to signal ratio.

6.2. *Sensitivity analysis*

In the engine tested in the present work, the skip-fire tests were available but in a standard test cell the equipment to perform such measurements is not usual, thus only motoring test are available. As previously discussed, the motoring tests have the drawback that they are performed with different thermodynamic conditions than combustion test, which can result in a lower quality of the HT adjustment. Thus, a sensitivity study was performed to evaluate the effect of the model parameters on the HT prediction quality.

The first term of Equation 6 indicates that the parameters affecting the tumble gas velocity model are the calibration constants (C_{t1} and C_{t2}), the characteristic gas velocity ($\bar{v}_m$) and the exponential function (f_w) parameters. According to Equation 8 the product $\eta_{tr}\dot{m}_a$ is the only uncertainty since A_{eff} and $\Delta\alpha_{IVO-IVC}$ are defined by the engine geometry, meanwhile the trapped mass is subject of experimental uncertainty, and additionally η_{tr} is not usually measured. In Equation 7, the constant a mathematically set, therefore only the exponent m and the angles α_0 and α_f can vary. It is important to remark that these three parameters cannot be adjusted simultaneously, since a different coefficient is related to different α_0 and α_f, thus in this study the exponent was kept constant and the angles were varied. In Equation 6 it is possible to observe that C_{t1} has almost the same effect as $\bar{v}_m$, being the unique difference its effect on C_{t2} due to the r_t ratio.

The sensitivity study is carried out to determine the parameter variation that produces a given uncertainty in the HT computation. Each parameter is swept to produce maximum variations of ±20% in the accumulated HT, with steps of ±5%. The results presented in Figure 11 indicates how the term $\eta_{tr}\dot{m}_a$ has a linear effect, and a variation of 1.4% in $\eta_{tr}\dot{m}_a$ results in a variation of 1% in Q_t. α_f shows also a linear trend, and a variation of 0.5° produces an uncertainty of 1% in Q_t, so the model is very sensitive to this parameter and it should be carefully calibrated. Finally α_0 has a different behaviour depending on its value: advancing α_0 about 1.5° results in a reduction of Q_t about 1% (being this trend linear), however delaying α_0 leads to a non-linear tend, thus a variation of 14° produces the maximum Q_t uncertainty of 5%, however a higher variation of α_0 produces lower Q_t uncertainty. This behaviour is explained by the instantaneous evolution of $\dot{Q}_t$ which is discuss later.

To analyse the instantaneous effect of each parameter on $\dot{Q}_t$, a reference well-adjusted test at 1200 rpm and Δp 400 mbar is compared with the HT resulting by considering the uncertainties of the parameters analysed in the previous paragraph. The results include in Figure 12 correspond to variations of ±10% on Q_t except in the case of delaying α_0, where the uncertainty in Q_t is 5%. $\dot{Q}_w$ is also presented in Figure 12, with the objective of highlight how in spite of the parameters variation, the qualitative fit of the proposed model is always better than the reference Woschni model. Some remarkable effects on the instantaneous HT profile are:

– Positive or negative variations of $\eta_{tr}\dot{m}_a$ affects directly the maximum HT reached, being the instantaneous difference more evident between 30° BTDC and 20° ATDC.

– Advancing α_0 has a moderate effect on the HT shape, while its effect on the maximum HT is higher. It is interesting to notice how advancing α_0 results in slightly more HT in the early compression stroke. It is explained by the higher tumble at this stage; however, at the beginning of compression, the pressure and temperature of the chamber are both low, thus the global effect on the HT is small. The tumble dissipation starts earlier, which results in a lower HT in the proximities of the TDC, which is not compensated by the small HT increase at the beginning of the compression stroke so the accumulated HT decreases.

– Delaying α_0 has a major effect on the HT shape, reducing significantly the HT at the beginning of the compression stroke since no tumble is considered until α_0, and increasing the HT close to the TDC. This HT increment close to TDC is compensated by the reduction at the beginning of compression, thus the mean HT uncertainty is constant (about 5%) as can be seen in the Figure 11. In spite of this moderate uncertainty, the main issue of delaying α_0 is the deformation of the $\dot{Q}_t$, which results in higher HT peaks but abnormally low HT in the compression stroke.

– The effect of α_f is observable between the maximum HT peak and the end of the tumble as can be seen in Figure 12. Delaying α_f results in a longer dissipation process, and hence higher HT. Consequently, advancing α_f has the contrary trend. The shape of $\dot{Q}_t$ is moderately affected by the variation of this parameter, but due to the cumulative effect on the mean HT, an accurate determination of α_f is important.

From this analysis, it can be concluded that the model is robust enough to be generally applied for engines with tumble, and it is robust against uncertainties of the parameters in a reasonable ranges, still performing better than the classical Woschni model, even including the effect of swirl, in terms of the instantaneous evolution and the mean HT determination.

7. Conclusions

A detailed HT model taking into account the gas velocity evolution caused by a high tumble movement is developed and validated. The model was developed in a research CI two-stroke engine with high tumble ratio and no swirl. The theoretical analysis was carried out by means of CFD simulations, whereas the calibration of the model was carried out by means of skip-fire tests. The most relevant conclusions are:

– The model presents a reduction of about 70% on the RMSE when comparing with the reference Woschni model. This improvement is observed for all the experimental conditions. The model also provides a better agreement with the experimental instantaneous HT, since it was observed that HT profile was well followed at different operating conditions.

– From the sensitivity analysis, the quantitative and qualitative effect of varying some parameters related with the gas velocity model were evaluated. The results show how variations of $\eta_{tr}\dot{m}_a$ about ±1.4%, advancing α_0 1.5° and varying α_f ±0.5° leads to 1% of uncertainty in Q_t.

– Retarding α_0 generates an uncertainty of about 5% in Q_t due to a compensation effect between the HT in the beginning of compression (low HT) and in the proximities of the TDC (high HT). However, the impact on the mean HT computation is moderate, while it has a remarkable effect in the instantaneous HT evolution.

It has been confirmed how the developed HT model is robust to be applied in engines with tumble movement. The model accounts for the spatially averaged gas velocity due to high tumble motion, and it allows to accurately determining its influence on the HT to the combustion chamber walls, which is critical to improve the quality of the combustion diagnosis models, widely used in the field of research and development.

8. Acknowledgements

The support of the Spanish Ministry of Economy and Competitiveness (TRA2013-41348-R) is greatly acknowledged.

The authors would like to thank RENAULT SAS for all the technical support provided to perform the research activities.

The authors want also to express their gratitude to CONVERGENT SCIENCE Inc. and IGNITE3D Engineering GmbH for their kind support for performing the CFD calculations using CONVERGE software.

References

[1] B. Mohan, W. Yang, S. K. Chou, Fuel injection strategies for performance improvement and emissions reduction in compression ignition engines-A review, Renewable and Sustainable Energy Reviews 28 (2013) 664-676. doi:10.1016/j.rser.2013.08.051.

[2] A. K. Agarwal, D. K. Srivastava, A. Dhar, R. K. Maurya, P. C. Shukla, A. P. Singh, Effect of fuel injection timing and pressure on combustion, emissions and performance characteristics of a single cylinder diesel engine, Fuel 111 (2013) 374-383. doi:10.1016/j.fuel.2013.03.016.

[3] S. Park, S. Yoon, C. Lee, Effects of multiple-injection strategies on overall spray behavior, combustion, and emissions reduction characteristics of biodiesel fuel, Applied Energy 88 (2011) 88-97. doi:10.1016/j.apenergy.2010.07.024.

[4] I. Al-Hinti, M. Samhouri, A. Al-Ghandoor, A. Sakhrieh, The effect of boost pressure on the performance characteristics of a diesel engine: a neuro-fuzzy approach, Applied Energy. 86 (2009) 113-121, doi:10.1016/j.apenergy.2008.04.015.

[5] Y. Park, C. Bae, Experimental study on the effects of high/low pressure EGR proportion in a passenger car diesel engine, Applied Energy 133 (2014) 308-316, doi:10.1016/j.apenergy.2014.08.003.

[6] G. Fontana, E. Galloni, Variable valve timing for fuel economy improvement in a small spark-ignition engine, Applied Energy 86 (1) (2009) 96-105. doi:10.1016/j.apenergy.2008.04.009.

[7] F. Perini, P. C. Miles, R. D. Reitz, A comprehensive modeling study of in-cylinder fluid flows in a high-swirl, light-duty optical diesel engine, Computers & Fluids 105 (2014) 113-124. doi:10.1016/j.compfluid.2014.09.011.

[8] S. Wei, F. Wang, X. Leng, X. Liu, K. Ji, Numerical analysis on the effect of swirl ratios on swirl chamber combustion system of DI diesel engines, Energy Conversion and Management 75 (2013) 184-190. doi:10.1016/j.enconman.2013.05.044.

[9] J. Benajes, R. Novella, D. De Lima, P. Tribotté, N. Quechon, P. Obernesser, V. Dugue, Analysis of the combustion process, pollutant emissions and efficiency of an innovative 2-stroke HSDI engine designed for automotive applications, Applied Thermal Engineering 58 (1-2) (2013) 181-193. doi:10.1016/j.applthermaleng.2013.03.050.

[10] T. Sandalcı, Y. Karagöz, Experimental investigation of the combustion characteristics, emissions and performance of hydrogen port fuel injection in a diesel engine, International Journal of Hydrogen Energy (2014) 1-10. doi:10.1016/j.ijhydene.2014.09.044.

[11] K. A. Sorate, P. V. Bhale, Biodiesel properties and automotive system compatibility issues, Renewable and Sustainable Energy Reviews 41 (2015) 777-798. doi:10.1016/j.rser.2014.08.079.

[12] V. Bermúdez, J.R. Serrano, P. Piqueras, O. García-Afonso, Pre-DPF water injection technique for pressure drop control in loaded wall-flow diesel particulate filters, Applied Energy 140 (2015) 234-245, doi:10.1016/j.apenergy.2014.12.003.

[13] Regulation (EU) No 333/2014 of the European Parliament and of the Council of 11 March 2014 amending Regulation (EC) No 443/2009 to define the modalities for reaching the 2020 target to reduce CO2 emissions from new passenger cars, Official Journal of the European Union L103 Vol 57 (2014) 15-21.

[14] S. Visakhamoorthy, T. Tzanetakis, D. Haggith, A. Sobiesiak, J. Z. Wen, Numerical study of a homogeneous charge compression ignition (HCCI) engine fueled with biogas, Applied Energy 92 (2012) 437-446, doi:10.1016/j.apenergy.2011.11.014.

[15] A. J. Torregrosa, A. Broatch, A. García, L. F. Mónico, Sensitivity of combustion noise and NOx and soot emissions to pilot injection in PCCI Diesel engines, Applied Energy 104 (2013) 149-157, doi:10.1016/j.apenergy.2012.11.040.

[16] T. Köfer, M. Lamping, A. Kolbeck, T. Genz, S. Pischinger, B. H, D. Adolph, The potential of downsizing Diesel engines considering performance and emissions challenges, IMechE (2008) 49-59.

[17] M. Thirouard, P. Pacaud, Increasing Power Density in HSDI Engines as an Approach for Engine Downsizing, SAE Int. J. Engines 3 (2) (2010) 56-71. doi: 10.4271/2010-01-1472.

[18] P. Tribotte, F. Ravet, V. Dugue, P. Obernesser, N. Quechon, J. Benajes, R. Novella, D. De Lima, Two Strokes Diesel Engine - Promising Solution to Reduce CO2 Emissions, Procedia - Social and Behavioral Sciences 48 (2012) 2295-2314. doi:10.1016/j.sbspro.2012.06.1202.

[19] J. Heywood, Internal Combustion Engines Fundamentals, McGraw-Hill, New York, 1988.

[20] J. Martín, Diagnóstico de la combustión en motores de Diesel de inyección directa, Reverté, Barcelona, 2012. ISBN: 978-84-291-4717-9

[21] F. Payri, P. Olmeda, J. Martín, R. Carreño, A New Tool to Perform Global Energy Balances in DI Diesel Engines, SAE Int. J. Engines 7(1) (2014). doi:10.4271/2014-01-0665.

[22] F. Payri, S. Molina, J. Martín, O. Armas, Influence of measurement errors and estimated parameters on combustion diagnosis, Applied Thermal Engineering 26 (2-3) (2006) 226-236. doi:10.1016/j.applthermaleng.2005.05.006.

[23] G. Woschni, A Universally Applicable Equation for the Instantaneous Heat Transfer Coefficient in the Internal Combustion Engine, SAE Technical Paper Series 670931.

[24] W. Annand, Heat transfer in the cylinders of reciprocating internal combustion engines, Proc. Inst. Mech. Engrs. 177 (1963) 973-990.

[25] G. Hohenberg, Experimentelle Erfassung derWandwarme in Kolbenmotoren, Ph.D. thesis, Technical University of Graz,Graz, Austria (1980).

[26] F. Payri, X. Margot, A. Gil, J. Martín, Computational Study of Heat Transfer to the Walls of a DI Diesel Engine, SAE Technical paper 2005-01-0210. doi:10.4271/2005-01-0210.

[27] A. Sanli, A. N. Ozsezen, I. Kilicaslan, M. Canakci, The influence of engine speed and load on the heat transfer between gases and in-cylinder walls at fired and motored conditions of an IDI diesel engine, Applied Thermal Engineering 28 (11-12) (2008) 1395-1404. doi:10.1016/j.applthermaleng.2007.10.005.

[28] N. Komninos, G. Kosmadakis, Heat transfer in HCCI multi-zone modeling: Validation of a new wall heat flux correlation under motoring conditions, Applied Energy 88 (5) (2011) 1635-1648. doi:10.1016/j.apenergy.2010.11.039.

[29] P. Tunestål, Self-tuning gross heat release computation for internal combustion engines, Control Engineering Practice 17 (4) (2009) 518-524. doi:10.1016/j.conengprac.2008.09.012.

[30] M. Achuth, P. S. Mehta, Predictions of tumble and turbulence in four-valve pentroof spark ignition engines, International Journal of Engine Research 2 (3) (2001) 209-227. doi:10.1243/1468087011545442.

[31] J. Maharudrppa Mallikarjuna, Effect of Manifold Orientation on Non-Reacting In-Cylinder Tumble Flows in an IC Engine with Pentroof Piston - An Investigation Using PIV, SAE paper 2010-01-0956. doi:10.4271/2010-01-0956.

[32] R. Huang, C. Huang, S. Chang, H. Yang, T. Lin, W. Hsu, Topological flow evolutions in cylinder of a motored engine during intake and compression strokes, Journal of Fluids and Structures 20 (1) (2005) 105-127. doi:10.1016/j.jfluidstructs.2004.09.002.

[33] M. Kim, S. Lee, W. Kim, Tumble Flow Measurements Using Three Different Methods and its Effects on Fuel Economy and Emissions, SAE Technical paper 2006-01-3345. doi:10.4271/2006-01-3345

[34] G. J. Micklow, W.-D. Gong, Investigation of the grid and intake-generated tumble on the in-cylinder flow in a compression ignition directinjection engine, Journal of Automobile Engineering 222 (5) (2008) 775-788. doi:10.1243/09544070JAUTO505.

[35] R. O. Grover Jr, D. Cleary, Correlating Measured Combustion Performance with CFD Predicted In-Cylinder Flows for a Spark-Ignition Direct-Injection (SIDI) Engine with Enhanced Charge Motion, SAE Technical paper 2013-01-1090. doi:10.4271/2013-01-1090.

[36] W. Dai, C. E. Newman, G. C. Davis, Predictions of In-Cylinder Tumble Flow and Combustion in SI Engines with a Quasi-Dimensional Model, SAE Technical Paper 961962.

[37] J. M. Pastor, Análisis del proceso de barrido en motores de dos tiempos de pequeña cilindrada, Reverté, Barcelona, 2009.

[38] J. B. Heywood, E. Sher, The Two-Stroke Cycle Engine: It's Development, Operation and Design, 1st Edition, SAE International, Taylor and Francis, Warrendale, Pennsylvania, 1999. ISBN:978-1560328315.

[39] G. Woschni, Die Berechnung der Wandverluste und der thermischen Belastung der Bauteile von Dieselmotoren., MTZ 31 (12) (1970) 491-499.

[40] H. Soyhan, H. Yasar, H. Walmsley, B. Head, G. Kalghatgi, C. Sorusbay, Evaluation of heat transfer correlations for HCCI engine modeling, Applied Thermal Engineering 29 (2-3) (2009) 541-549. doi:10.1016/j.applthermaleng.2008.03.014.

[41] D. Olsen, G. Hutcherson, B. Willson, C. Mitchell, Development of the tracer gas method for large bore natural gas engines: part 1 - method validation, J. Eng. Gas Turbines Power 124 (3) (2002) 678-685. doi:10.1115/1.1454116.

[42] D. Olsen, G. Hutcherson, B. Willson, C. Mitchell, Development of the tracer gas method for large bore natural gas engines: part 2 - measurement of scavenging parameters, J. Eng. Gas Turbines Power 124 (3) (2002) 686-694. doi:10.1115/1.1454117.

[43] M. Lapuerta, O. Armas, J. J. Hernández, Diagnosis of DI Diesel combustion from in-cylinder pressure signal by estimation of mean thermodynamic properties of the gas, Applied Thermal Engineering 19 (5) (1999) 513-529. doi:10.1016/S1359-4311(98)00075-1.

[44] T. Morel, R. Keribar, Heat radiation in DI Diesel engines, SAE Technical Paper 860445.

[45] J.J. Lopez, J.M. Garcia-Oliver, J. Martin, J.P. Chemisky, A. Bouet, A soot radiation model for diesel sprays, SAE Technical paper 2012-01-1069, doi:10.4271/2012-01-1069.

[46] A. J. Torregrosa, P. Olmeda, B. Degraeuwe, M. Reyes, A concise wall temperature model for DI Diesel engines, Applied Thermal Engineering 26 (11-12) (2006) 1320-1327. doi:10.1016/j.applthermaleng.2005.10.021.

[47] A. J. Torregrosa, A. Broatch, P. Olmeda, J. Martín, A contribution to film coefficient estimation in piston cooling galleries, Experimental Thermal and Fluid Science 34 (2) (2010) 142-151. doi:10.1016/j.expthermflusci.2009.10.003.

[48] J. Benajes, P. Olmeda, J. Martín, R. Carreño, A new methodology for uncertainties characterization in combustion diagnosis and thermodynamic modelling, Applied Thermal Engineering 71 (2014) 389-399. doi:10.1016/j.applthermaleng.2014.07.010.

9. Figures

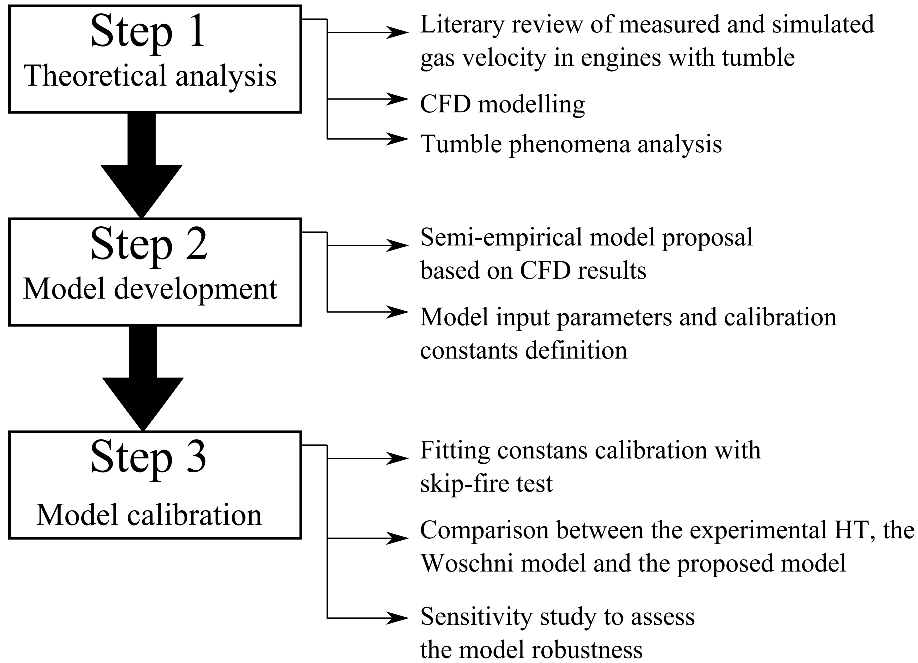

Figure 1: Procedure Scheme

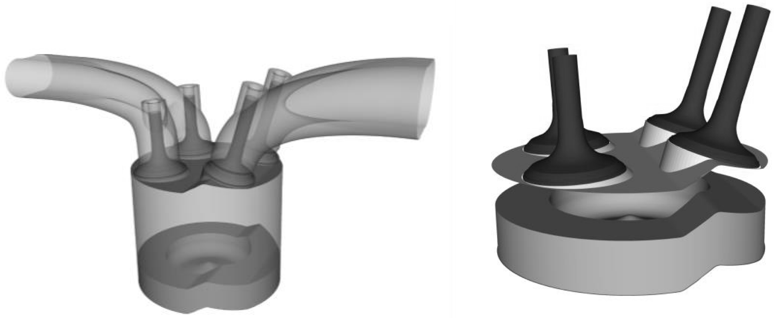

Figure 2: Sketch of the cylinder head designed for the 2-stroke engine architecture (Patent Renault FR2931880)

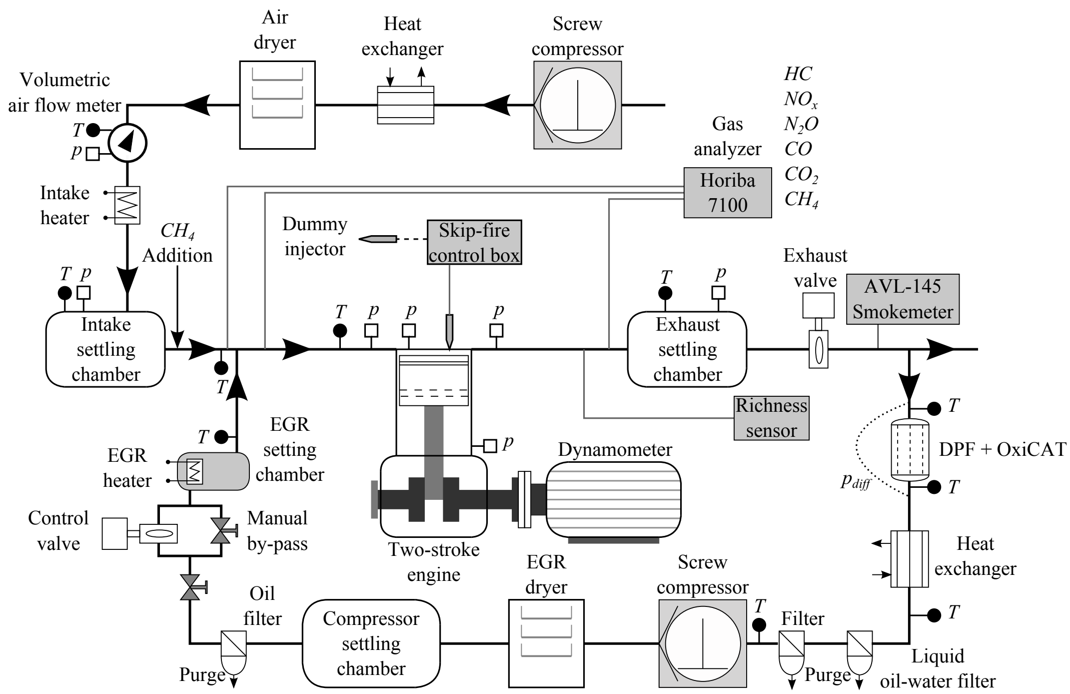

Figure 3: Engine test cell scheme

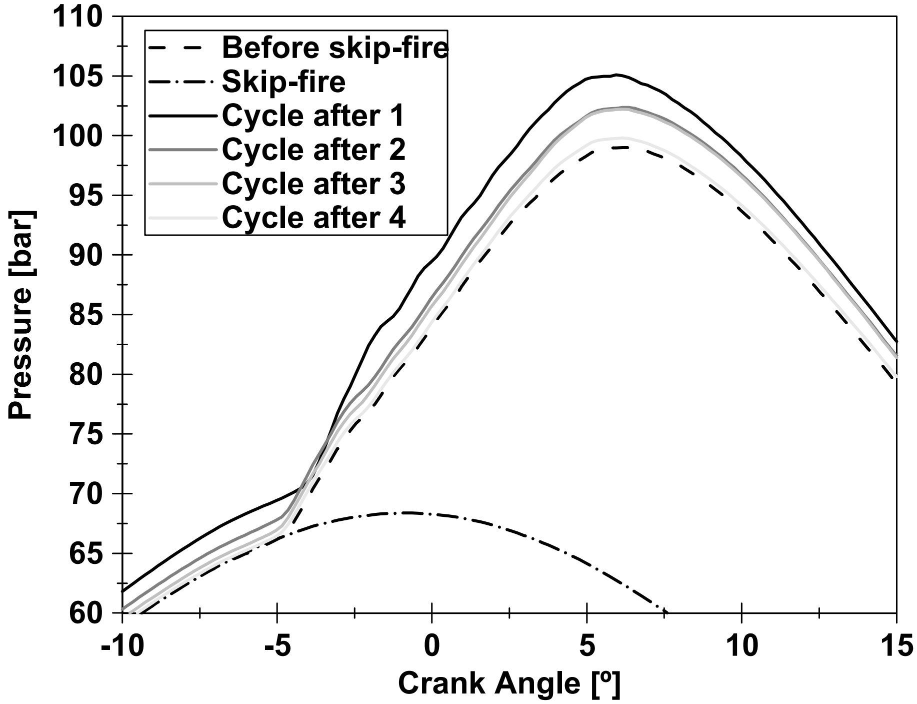

Figure 4: Skip-fire pressure

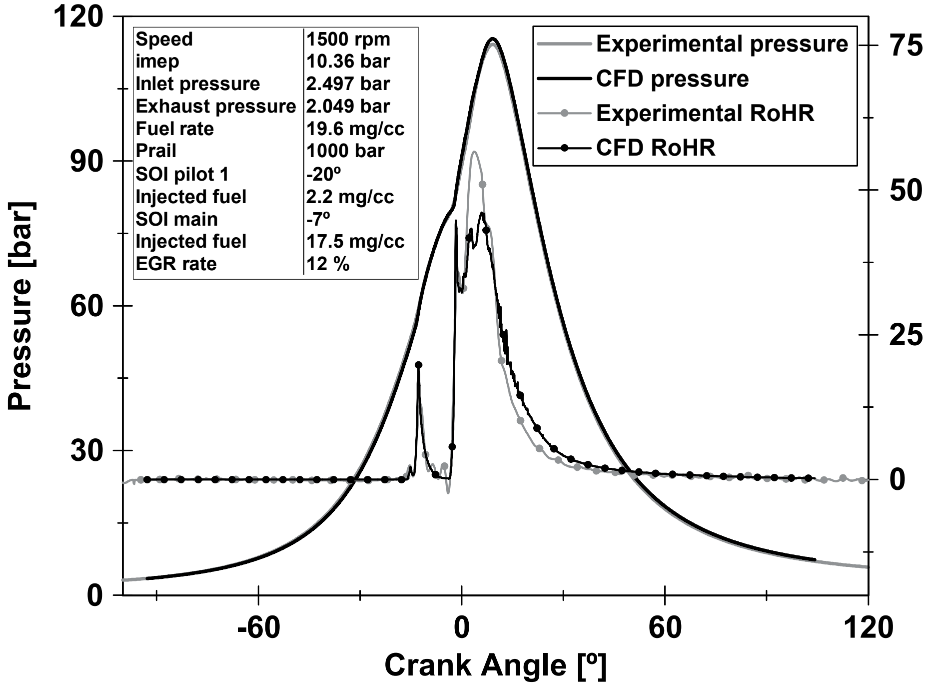

Figure 5: CFD validation

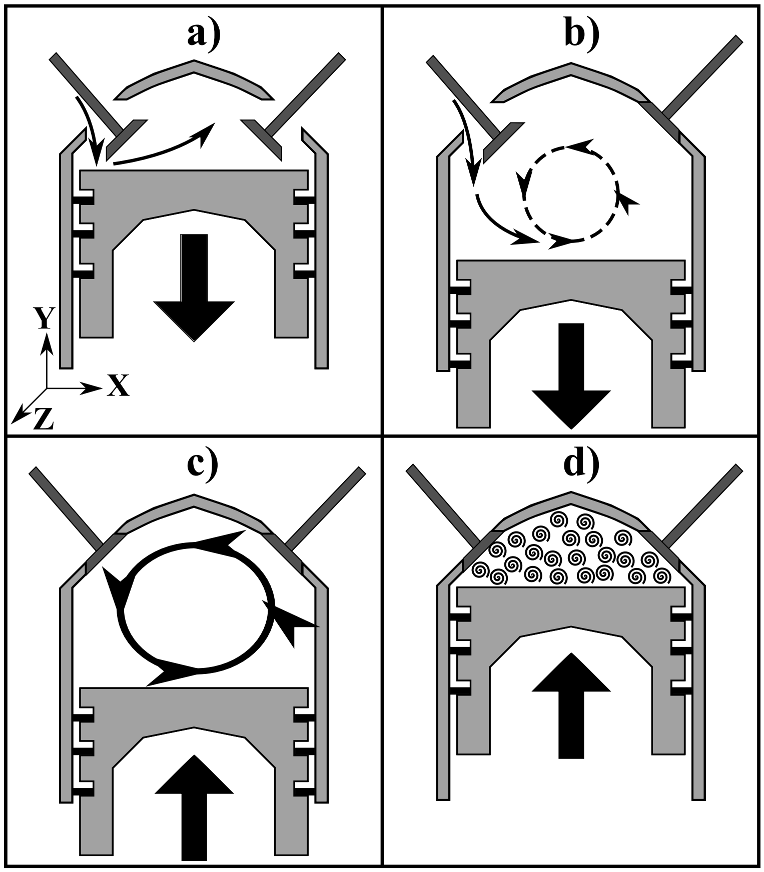

Figure 6: Main process of tumble evolution

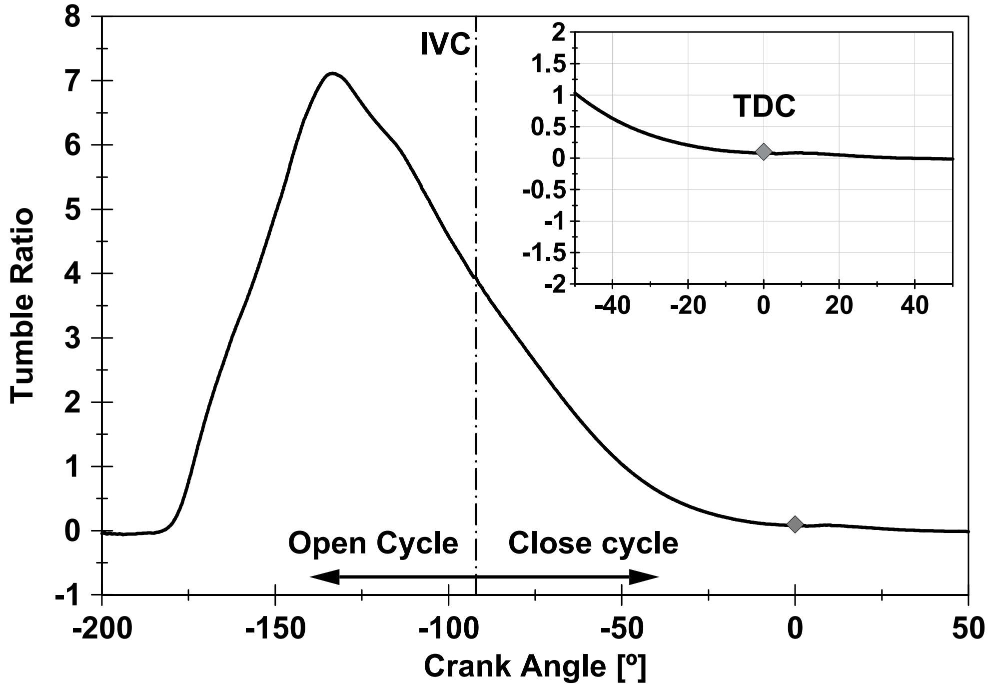

Figure 7: Tumble ratio evolution in a perpendicular plane of the cylinder axis

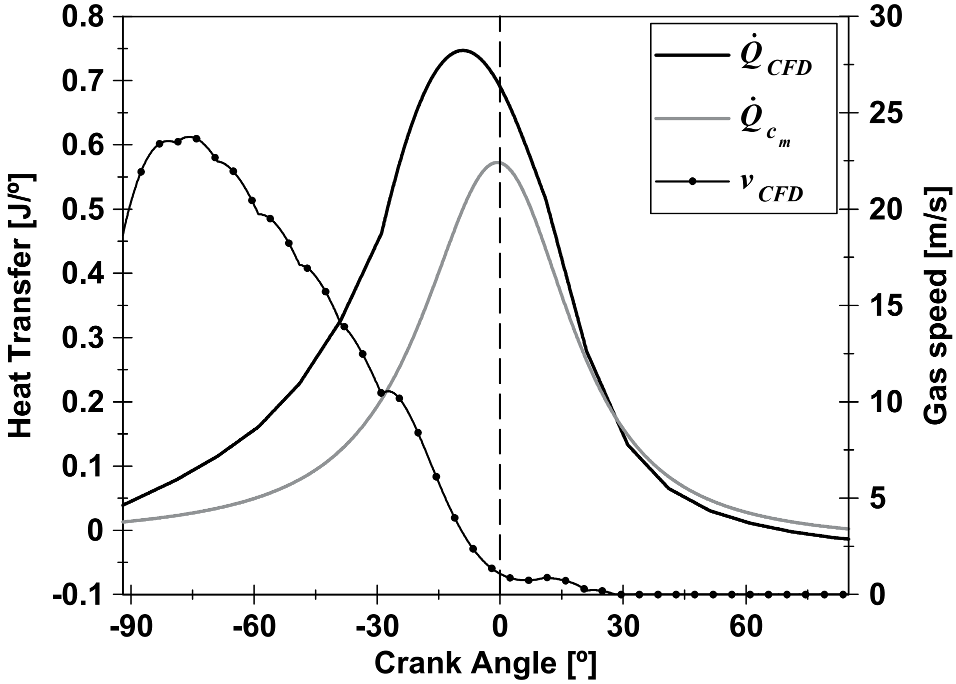

Figure 8: CFD HT and tumble gas velocity

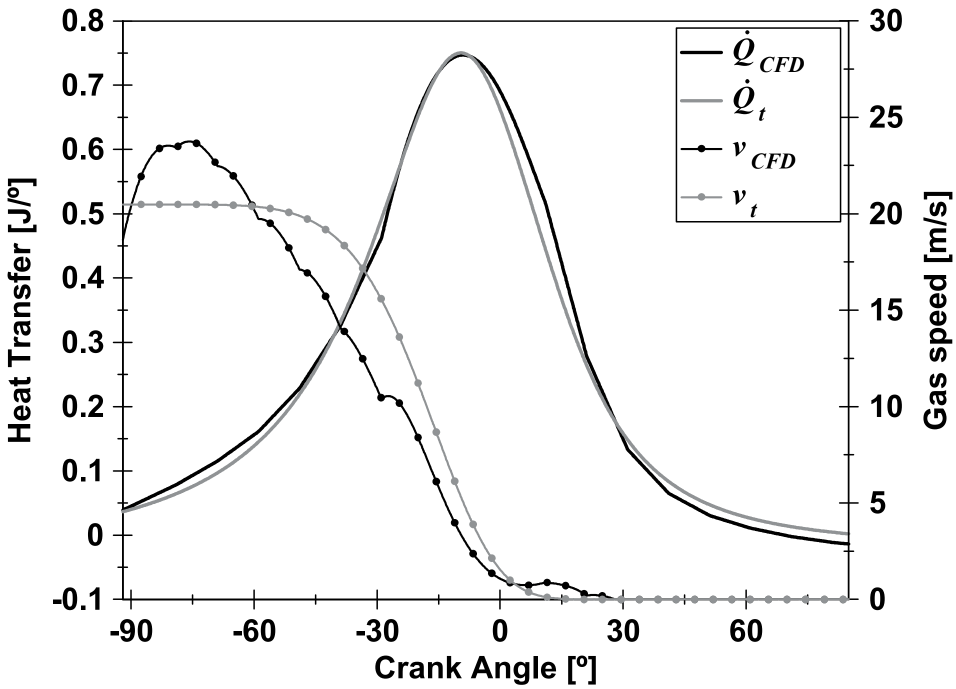

Figure 9: Tumble gas velocity model

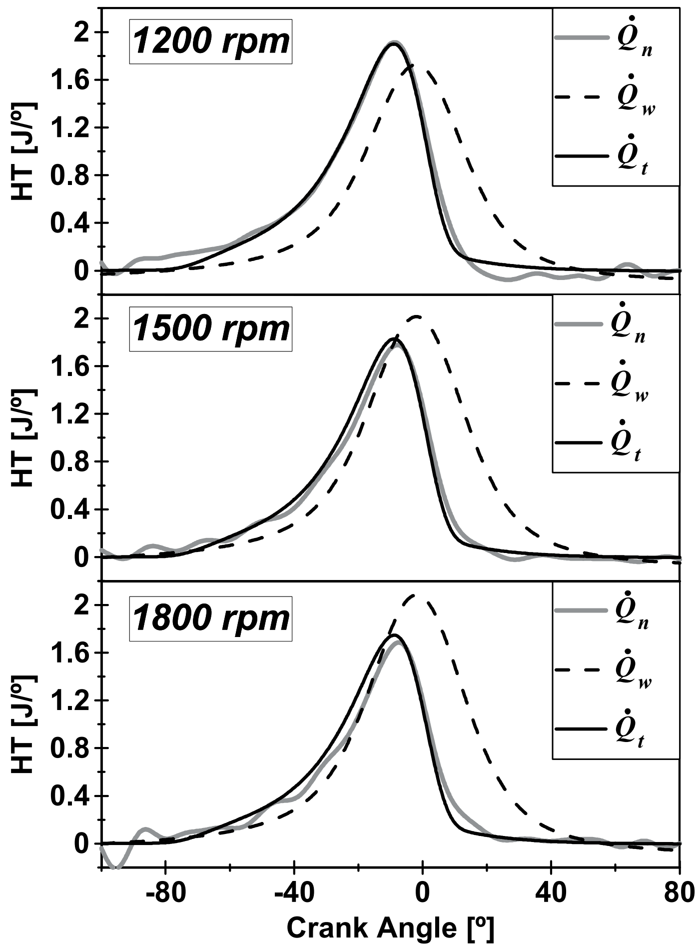

Figure 10: Heat transfer comparison ($\Delta p = 400mbar$)

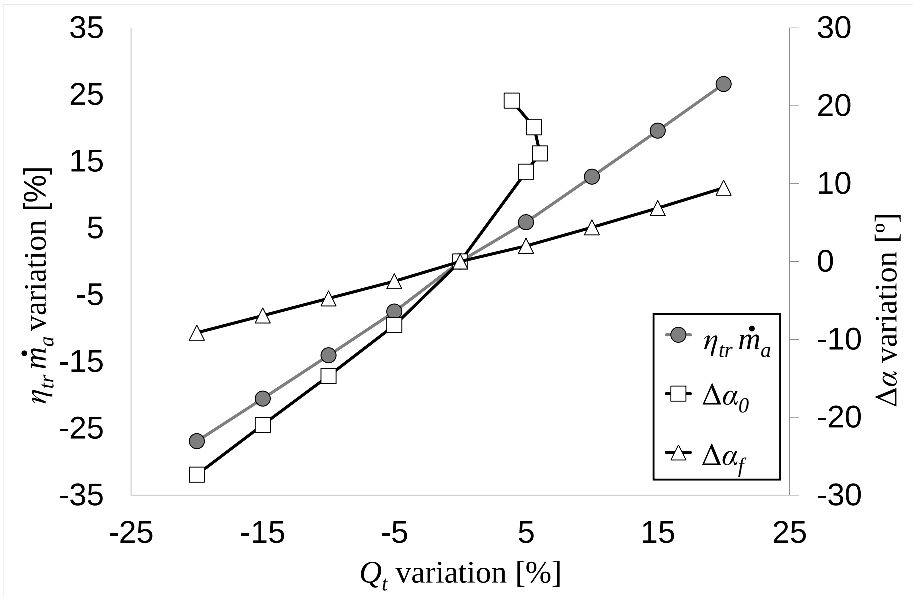

Figure 11: Sensitivity analysis

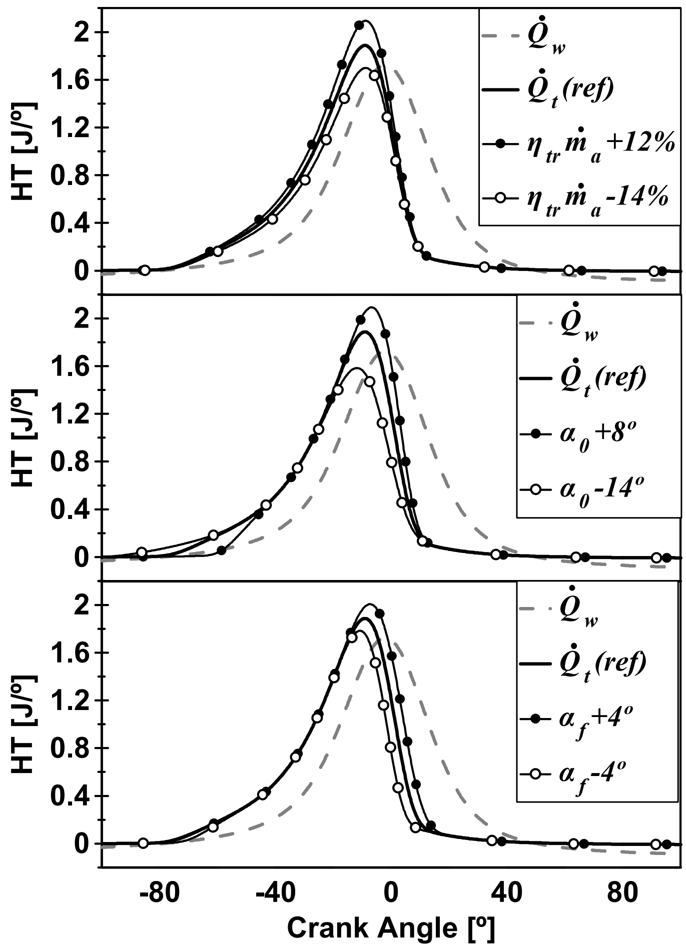

Figure 12: HT sensitivity at 1200 rpm and Δp = 400$mbar$

10. Tables

Table 1: Main engine geometrical characteristics

Displacement	365 cm^3
Bore	76 mm
Stroke	80.5 mm
Connecting rod length	133.75 mm
Geometric CR	17.8
Number of valves/cylinder	4
Type of scavenge	Poppet valves with scavenge loop
Intake camshaft profile	Duration: 80°/max. lift: 6 mm
Exhaust camshaft definition	Duration : 90°/max. lift: 8.5 mm

Table 2: Measured operational points

Speed	Δp	$imep$	Air mass flow rate	η_{tr}
[rpm]	[mbar]	[bar]	[g/s]	[%]
1200	300	3.7	7.4	69
1200	400	5.6	10.1	72
1200	500	7.5	12.2	84
1500	300	3.7	9.6	78
1500	400	5.6	11.0	79
1500	500	7.5	13.4	79
1800	300	3.7	8.7	80
1800	400	5.6	11.4	84
1800	500	7.5	14.7	85

Table 3: CFD emissions validation

	CFD	Experiment
CO	2,2017 mg/s	3,7500 mg/s
soot	0,0565 mg/s	0,0670 mg/s
HC	0,0032 mg/s	0,3000 mg/s
NO_x	5,4780 mg/s	5,9000 mg/s

Table 4: Model adjusted parameters

Parameter	Value
m	6
a	-6.907
α_0	34.15° BTDC
α_f	14.9° ATDC
C_{t1}	0.804
C_{t2}	1.293
r_t	0.622

Table 5: RMSE of the HT computation by using the Woschni model and the proposed model

Speed (rmp)	Δp (mbar)	Q_w RMSE (J/°)	Q_t RMSE (J/°)	Improvement (%)
1200	300	0.30	0.09	70
1200	400	0.33	0.08	77
1200	500	0.38	0.10	74
1500	300	0.31	0.08	75
1500	400	0.30	0.07	76
1500	500	0.31	0.12	61
1800	300	0.28	0.05	82
1800	400	0.28	0.08	72
1800	500	0.31	0.18	41